

SWIFT AND FERMI OBSERVATIONS OF THE EARLY AFTERGLOW OF THE SHORT GAMMA-RAY BURST 090510

- M. DE PASQUALE^{1,66}, P. SCHADY¹, N. P. M. KUIN¹, M. J. PAGE^{1,66}, P. A. CURRAN¹, S. ZANE¹, S. R. OATES¹, S. T. HOLLAND²,
A. A. BREEVELD¹, E. A. HOVERSTEN³, G. CHINCARINI^{4,5}, D. GRUPE³, A. A. ABDO^{6,7}, M. ACKERMANN⁸, M. AJELLO⁸,
M. AXELSSON^{9,10}, L. BALDINI¹¹, J. BALLE¹², G. BARBIELLINI^{13,14}, M. G. BARING¹⁵, D. BASTIERI^{16,17}, K. BECHTOL⁸,
R. BELLAZZINI¹¹, B. BERENJI⁸, E. BISSALDI¹⁸, R. D. BLANDFORD⁸, E. D. BLOOM⁸, E. BONAMENTE^{19,20}, A. W. BORGLAND⁸,
A. BOUVIER⁸, J. BREGEON¹¹, A. BREZ¹¹, M. S. BRIGGS²¹, M. BRIGIDA^{22,23}, P. BRUEL²⁴, T. H. BURNETT²⁵, S. BUSON¹⁷,
G. A. CALIANDRO²⁶, R. A. CAMERON⁸, P. A. CARAVEO²⁷, S. CARRIGAN¹⁷, J. M. CASANDJIAN¹², C. CECCHI^{19,20}, Ö. ÇELİK^{2,28,29},
A. CHEKHTMAN^{6,30}, J. CHIANG⁸, S. CIPRINI²⁰, R. CLAUS⁸, J. COHEN-TANUGI³¹, V. CONNAUGHTON²¹, J. CONRAD^{10,32,64},
C. D. DERMER⁶, A. DE ANGELIS³³, F. DE PALMA^{22,23}, B. L. DINGUS³⁴, E. DO COUTO E SILVA⁸, P. S. DRELL⁸, R. DUBOIS⁸,
D. DUMORA^{35,36}, C. FARNIER³¹, C. FAVUZZI^{22,23}, S. J. FEGAN²⁴, G. FISHMAN³⁷, W. B. FOCKE⁸, M. FRAILIS³³, Y. FUKAZAWA³⁸,
S. FUNK⁸, P. FUSCO^{22,23}, F. GARGANO²³, D. GASPARRINI³⁹, N. GEHRELS^{2,3,40}, S. GERMANI^{19,20}, N. GIGLIETTO^{22,23},
F. GIORDANO^{22,23}, T. GLANZMAN⁸, G. GODFREY⁸, J. GRANOT⁴¹, J. GREINER¹⁸, I. A. GRENIER¹², J. E. GROVE⁶, L. GUILLEMOT⁴²,
S. GUIRIEC²¹, A. K. HARDING², M. HAYASHIDA⁸, E. HAYS², D. HORAN²⁴, R. E. HUGHES⁴³, M. S. JACKSON^{10,44}, G. JÓHANNESSON⁸,
A. S. JOHNSON⁸, W. N. JOHNSON⁶, T. KAMAE⁸, H. KATAGIRI³⁸, J. KATAOKA⁴⁵, N. KAWAI^{46,47}, M. KERR²⁵, R. M. KIPPEN³⁴,
J. KNÖDLSER⁴⁸, D. KOCEVSKI⁸, M. KUSS¹¹, J. LANDE⁸, L. LATRONICO¹¹, M. LEMOINE-GOUMARD^{35,36}, F. LONGO^{13,14},
F. LOPARCO^{22,23}, B. LOTT^{35,36}, M. N. LOVELLETTE⁶, P. LUBRANO^{19,20}, A. MAKEEV^{6,30}, M. N. MAZZIOTTA²³, J. E. MCENERY^{2,40},
S. MCGLYNN^{10,44}, C. MEEGAN⁴⁹, P. MÉSZÁROS³, C. MEURER^{10,32}, P. F. MICHELSON⁸, W. MITTHUMSIRI⁸, T. MIZUNO³⁸,
C. MONTE^{22,23}, M. E. MONZANI⁸, E. MORETTI^{13,14}, A. MORSELLI⁵⁰, I. V. MOSKALENKO⁸, S. MURGIA⁸, P. L. NOLAN⁸,
J. P. NORRIS⁵¹, E. NUSS³¹, M. OHNO⁵², T. OHSUGI³⁸, N. OMODEI¹¹, E. ORLANDO¹⁸, J. F. ORMES⁵¹, W. S. PACIESAS²¹, D. PANEQUE⁸,
J. H. PANETTA⁸, D. PARENT^{35,36}, V. PELASSA^{31,66}, M. PEPE^{19,20}, M. PESCE-ROLLINS¹¹, F. PIRON³¹, T. A. PORTER⁵³, R. PREECE²¹,
S. RAINÒ^{22,23}, R. RANDO^{16,17}, M. RAZZANO¹¹, A. REIMER^{8,54}, O. REIMER^{8,54}, T. REPOSEUR^{35,36}, S. RITZ⁵³, L. S. ROCHESTER⁸,
A. Y. RODRIGUEZ²⁶, M. ROTH²⁵, F. RYDE^{10,44}, H. F.-W. SADROZINSKI⁵³, A. SANDER⁴³, P. M. SAZ PARKINSON⁵³, J. D. SCARGLE⁵⁵,
T. L. SCHALK⁵³, C. SGRÒ¹¹, E. J. SISKIND⁵⁶, P. D. SMITH⁴³, G. SPANDRE¹¹, P. SPINELLI^{22,23}, M. STAMATIKOS^{2,43}, J.-L. STARCK¹²,
F. W. STECKER², M. S. STRICKMAN⁶, D. J. SUSON⁵⁷, H. TAJIMA⁸, H. TAKAHASHI³⁸, T. TANAKA⁸, J. B. THAYER⁸, J. G. THAYER⁸,
D. J. THOMPSON², L. TIBALDO^{16,17,12}, K. TOMA^{3,66}, D. F. TORRES^{26,58}, G. TOSTI^{19,20}, A. TRAMACERE^{8,59}, Y. UCHIYAMA⁸,
T. UEHARA³⁸, T. L. USHER⁸, A. J. VAN DER HORST^{37,65}, V. VASILEIOU^{28,29}, N. VILCHEZ⁴⁸, V. VITALE^{50,60}, A. VON KIENLIN¹⁸,
A. P. WAITE⁸, P. WANG⁸, B. L. WINER⁴³, K. S. WOOD⁶, X. F. WU^{3,61,62}, R. YAMAZAKI³⁸, T. YLINEN^{10,44,63}, AND M. ZIEGLER⁵³
- ¹ Mullard Space Science Laboratory, University College London, Holmbury St. Mary, Dorking Surrey, RH5 6NT, UK; mdp@mssl.ucl.ac.uk, mjp@mssl.ucl.ac.uk
² NASA Goddard Space Flight Center, Greenbelt, MD 20771, USA
³ Department of Astronomy and Astrophysics, Pennsylvania State University, University Park, PA 16802, USA; toma@astro.psu.edu
⁴ Università degli Studi di Milano Bicocca, Piazza della Scienza, 3, 20126 Milano, Italy
⁵ Osservatorio Astronomico di Brera (INAF), Via E. Bianchi 46, 23807 Merate (LC), Italy
⁶ Space Science Division, Naval Research Laboratory, Washington, DC 20375, USA
⁷ National Research Council Research Associate, National Academy of Sciences, Washington, DC 20001, USA
⁸ W. W. Hansen Experimental Physics Laboratory, Kavli Institute for Particle Astrophysics and Cosmology, Department of Physics and SLAC National Accelerator
Laboratory, Stanford University, Stanford, CA 94305, USA
⁹ Department of Astronomy, Stockholm University, SE-106 91 Stockholm, Sweden
¹⁰ The Oskar Klein Centre for Cosmoparticle Physics, AlbaNova, SE-106 91 Stockholm, Sweden
¹¹ Istituto Nazionale di Fisica Nucleare, Sezione di Pisa, I-56127 Pisa, Italy
¹² Laboratoire AIM, CEA-IRFU/CNRS/Université Paris Diderot, Service d'Astrophysique, CEA Saclay, 91191 Gif sur Yvette, France
¹³ Istituto Nazionale di Fisica Nucleare, Sezione di Trieste, I-34127 Trieste, Italy
¹⁴ Dipartimento di Fisica, Università di Trieste, I-34127 Trieste, Italy
¹⁵ Rice University, Department of Physics and Astronomy, MS-108, P.O. Box 1892, Houston, TX 77251, USA
¹⁶ Istituto Nazionale di Fisica Nucleare, Sezione di Padova, I-35131 Padova, Italy
¹⁷ Dipartimento di Fisica "G. Galilei," Università di Padova, I-35131 Padova, Italy
¹⁸ Max-Planck Institut für extraterrestrische Physik, 85748 Garching, Germany
¹⁹ Istituto Nazionale di Fisica Nucleare, Sezione di Perugia, I-06123 Perugia, Italy
²⁰ Dipartimento di Fisica, Università degli Studi di Perugia, I-06123 Perugia, Italy
²¹ Center for Space Plasma and Aeronomic Research (CSPAR), University of Alabama in Huntsville, Huntsville, AL 35899, USA
²² Dipartimento di Fisica "M. Merlin" dell'Università e del Politecnico di Bari, I-70126 Bari, Italy
²³ Istituto Nazionale di Fisica Nucleare, Sezione di Bari, 70126 Bari, Italy
²⁴ Laboratoire Leprince-Ringuet, École polytechnique, CNRS/IN2P3, Palaiseau, France
²⁵ Department of Physics, University of Washington, Seattle, WA 98195-1560, USA
²⁶ Institut de Ciències de l'Espai (IEEC-CSIC), Campus UAB, 08193 Barcelona, Spain
²⁷ INAF-Istituto di Astrofisica Spaziale e Fisica Cosmica, I-20133 Milano, Italy
²⁸ Center for Research and Exploration in Space Science and Technology (CRESST) and NASA Goddard Space Flight Center, Greenbelt, MD 20771, USA
²⁹ Department of Physics and Center for Space Sciences and Technology, University of Maryland Baltimore County, Baltimore, MD 21250, USA
³⁰ George Mason University, Fairfax, VA 22030, USA
³¹ Laboratoire de Physique Théorique et Astroparticules, Université Montpellier 2, CNRS/IN2P3, Montpellier, France; Veronique.Pelassa@lpta.in2p3.fr
³² Department of Physics, Stockholm University, AlbaNova, SE-106 91 Stockholm, Sweden
³³ Dipartimento di Fisica, Università di Udine and Istituto Nazionale di Fisica Nucleare, Sezione di Trieste, Gruppo Collegato di Udine, I-33100 Udine, Italy
³⁴ Los Alamos National Laboratory, Los Alamos, NM 87545, USA
³⁵ CNRS/IN2P3, Centre d'Études Nucléaires Bordeaux Gradignan, UMR 5797, Gradignan, 33175, France

- ³⁶ Centre d'Études Nucléaires Bordeaux Gradignan, Université de Bordeaux, UMR 5797, Gradignan 33175, France
- ³⁷ NASA Marshall Space Flight Center, Huntsville, AL 35812, USA
- ³⁸ Department of Physical Sciences, Hiroshima University, Higashi-Hiroshima, Hiroshima 739-8526, Japan
- ³⁹ Agenzia Spaziale Italiana (ASI) Science Data Center, I-00044 Frascati (Roma), Italy
- ⁴⁰ Department of Physics and Department of Astronomy, University of Maryland, College Park, MD 20742, USA
- ⁴¹ Centre for Astrophysics Research, University of Hertfordshire, College Lane, Hatfield AL10 9AB, UK
- ⁴² Max-Planck-Institut für Radioastronomie, Auf dem Hügel 69, 53121 Bonn, Germany
- ⁴³ Department of Physics, Center for Cosmology and Astro-Particle Physics, The Ohio State University, Columbus, OH 43210, USA
- ⁴⁴ Department of Physics, Royal Institute of Technology (KTH), AlbaNova, SE-106 91 Stockholm, Sweden
- ⁴⁵ Waseda University, 1-104 Totsukamachi, Shinjuku-ku, Tokyo 169-8050, Japan
- ⁴⁶ Department of Physics, Tokyo Institute of Technology, Meguro City, Tokyo 152-8551, Japan
- ⁴⁷ Cosmic Radiation Laboratory, Institute of Physical and Chemical Research (RIKEN), Wako, Saitama 351-0198, Japan
- ⁴⁸ Centre d'Étude Spatiale des Rayonnements, CNRS/UPS, BP 44346, F-30128 Toulouse Cedex 4, France
- ⁴⁹ Universities Space Research Association (USRA), Columbia, MD 21044, USA
- ⁵⁰ Istituto Nazionale di Fisica Nucleare, Sezione di Roma "Tor Vergata," I-00133 Roma, Italy
- ⁵¹ Department of Physics and Astronomy, University of Denver, Denver, CO 80208, USA
- ⁵² Institute of Space and Astronautical Science, JAXA, 3-1-1 Yoshinodai, Sagami-hara, Kanagawa 229-8510, Japan
- ⁵³ Santa Cruz Institute for Particle Physics, Department of Physics and Department of Astronomy and Astrophysics, University of California at Santa Cruz, Santa Cruz, CA 95064, USA
- ⁵⁴ Institut für Astro- und Teilchenphysik and Institut für Theoretische Physik, Leopold-Franzens-Universität Innsbruck, A-6020 Innsbruck, Austria
- ⁵⁵ Space Sciences Division, NASA Ames Research Center, Moffett Field, CA 94035-1000, USA
- ⁵⁶ NYCB Real-Time Computing Inc., Lattingtown, NY 11560-1025, USA
- ⁵⁷ Department of Chemistry and Physics, Purdue University Calumet, Hammond, IN 46323-2094, USA
- ⁵⁸ Institutió Catalana de Recerca i Estudis Avançats (ICREA), Barcelona, Spain
- ⁵⁹ Consorzio Interuniversitario per la Fisica Spaziale (CIFS), I-10133 Torino, Italy
- ⁶⁰ Dipartimento di Fisica, Università di Roma "Tor Vergata," I-00133 Roma, Italy
- ⁶¹ Joint Center for Particle Nuclear Physics and Cosmology (J-CPNPC), Nanjing 210093, China
- ⁶² Purple Mountain Observatory, Chinese Academy of Sciences, Nanjing 210008, China
- ⁶³ School of Pure and Applied Natural Sciences, University of Kalmar, SE-391 82 Kalmar, Sweden
- Received 2009 October 9; accepted 2009 December 10; published 2010 January 14*

ABSTRACT

We present the observations of GRB090510 performed by the *Fermi* Gamma-Ray Space Telescope and the *Swift* observatory. This is a bright, short burst that shows an extended emission detected in the GeV range. Furthermore, its optical emission initially rises, a feature so far observed only in long bursts, while the X-ray flux shows an initial shallow decrease, followed by a steeper decay. This exceptional behavior enables us to investigate the physical properties of the gamma-ray burst outflow, poorly known in short bursts. We discuss internal and external shock models for the broadband energy emission of this object.

Key words: gamma-ray burst: individual (GRB090510) – relativistic processes – shock waves

1. INTRODUCTION

With the availability of a relatively large sample of gamma-ray bursts (GRBs), we came to recognize that they comprise two large classes (Kouveliotou et al. 1993): the so-called short-hard GRBs (duration $\lesssim 2$ s) and the long-soft ones ($\gtrsim 2$ s). There is now increasing consensus that the observed dichotomy among long/short GRBs may indicate diverse initial physical conditions and progenitors. Long GRBs are associated with the demise of massive stars (Ferrero et al. 2006). Instead, short GRBs often occur in early-type galaxies (Zhang et al. 2009; Gehrels et al. 2009; Fong et al. 2010). This supports their interpretation in terms of compact object mergers.

Crucial information on GRBs is revealed by their afterglows, which can be monitored by *Swift* (Gehrels et al. 2004) in the optical and the X-ray range as early as ~ 100 s after the burst. In this Letter, we present the study of the short GRB090510 with *Swift* and *Fermi* in a broad energy range, which extends from the optical up to a few GeV.

We report our observations and analysis in Section 2. In Section 3, we propose two different interpretations, and in Section 4 we draw our conclusions. Hereafter, we use the

conventions $X = 10^n X_n$ for cgs units and $F \propto t^{-\alpha} \nu^{-\beta}$, where F is the energy flux, t is time from the trigger of *Swift* Burst Alert Telescope (BAT; Barthelmy et al. 2005a), and ν is the frequency. Errors are reported at 1σ , unless otherwise specified. We assume a cosmology in which $H_0 = 71$ km s $^{-1}$ Mpc $^{-1}$, $\Omega_m = 0.27$, $\Omega_\lambda = 0.73$ (Spergel et al. 2003). All the fluxes, times, and frequencies are measured in the observer's frame.

2. OBSERVATIONS AND DATA ANALYSIS

2.1. BAT Data

At 00:23:00 UT, 2009 May 10, BAT, which operates in the 15–350 keV range, triggered on GRB090510 (Hoversten et al. 2009). *Swift* slewed immediately to the burst. The duration was $T_{90} = 0.30 \pm 0.07$ s. A detailed analysis of the BAT data is shown in Ukwatta et al. (2009).

2.2. XRT Data

The *Swift* X-ray Telescope (XRT; 0.3–10 keV; Burrows et al. 2005) began observing the X-ray afterglow of GRB090510 at T+98 s. The light curve (Figure 1) shows an initial slow flux decline. Observations were interrupted when the source entered the Earth constraint at T+1.9 ks. When they resumed, at T+5.1 ks, the flux was much lower. A broken power-law fit of the light curve gives as best-fit parameters an early decay slope $\alpha_{X,1} = 0.74 \pm 0.03$, break time $t_X = 1.43^{+0.09}_{-0.15}$ ks, late

⁶⁴ Royal Swedish Academy of Sciences Research Fellow, funded by a grant from the K. A. Wallenberg Foundation.

⁶⁵ NASA Postdoctoral Program Fellow, USA.

⁶⁶ Corresponding authors.

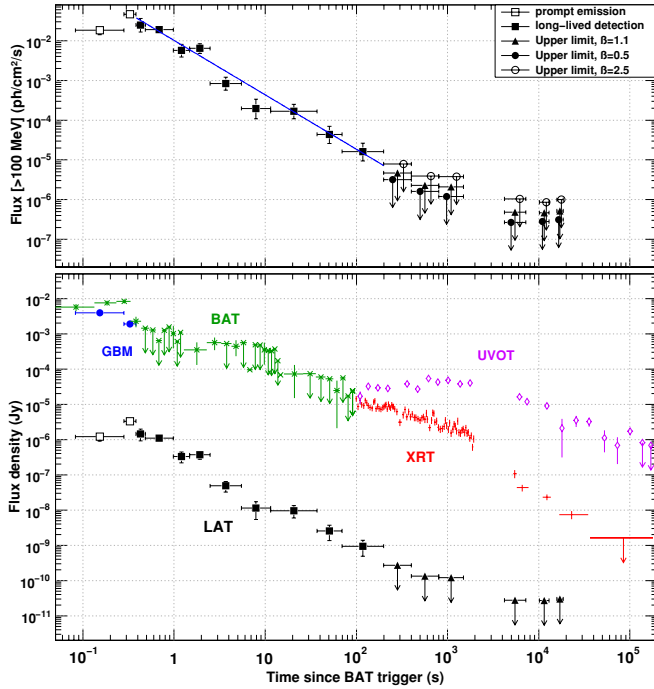


Figure 1. Top: LAT flux above 100 MeV and best fit to the flux decay (line). Bottom: energy flux densities averaged in the observed energy bands: BAT (15–350 keV, stars); XRT (0.2–10 keV, crosses); UVOT renormalized to white (diamonds); LAT (100 MeV–4 GeV, filled squares; the average spectral index was used to convert from photon to energy flux) with upper limits for $\beta = 1.1$ (triangles). The prompt emission is shown for comparison: GBM (8 keV–1 MeV, circles), LAT (100 MeV–4 GeV, empty squares). XRT light curve is obtained as in Evans et al. (2007, 2009). All data are shown with 68% error bars or 95% confidence level upper limits.

decay slope $\alpha_{X,2} = 2.18 \pm 0.10$; $\chi^2 = 112$ with 77 degrees of freedom (dof), which is still marginally acceptable (chance probability $P = 0.0054$).

2.3. UVOT and Other Optical Data

The *Swift* Ultra Violet and Optical Telescope (UVOT; 160–800 nm; Roming et al. 2005; Poole et al. 2008) began settled exposures at T+97 s. The light curve of the optical afterglow, produced by renormalizing all individual filters to white, as described in Oates et al. (2009), is shown in Figure 1. The optical emission rises until ~ 1.6 ks, then decays. The optical light curve is well fitted ($\chi^2/\text{dof} = 23.9$) by a broken power law (Beuermann et al. 1999) with a smooth break. The best-fit parameters are $\alpha_{\text{Opt},1} = -0.50^{+0.11}_{-0.13}$; $t_{\text{peak}} = 1.58^{+0.46}_{-0.37}$ ks; $\alpha_{\text{Opt},2} = 1.13^{+0.11}_{-0.10}$. Adding a constant does not improve the fit significantly, suggesting a small host galaxy contribution. Very Large Telescope observations (Rau et al. 2009) provide a spectroscopic redshift of $z = 0.903$. Using this redshift and the *Fermi* spectral parameters, the isotropic equivalent energy of GRB090510 is $E_{\text{iso}} = 1.08 \times 10^{53}$ erg in the 10 keV–30 GeV rest frame (A. A. Abdo et al. 2010, in preparation).

2.4. Fermi Data

GRB090510 triggered both instruments on board the *Fermi* observatory (Guiriec et al. 2009; Ohno & Pelassa 2009). The Gamma-ray Burst Monitor (GBM; 8 keV–40 MeV) observed the burst during the prompt emission phase, and an autonomous repointing enabled the Large Area Telescope (LAT; 20 MeV–more than 300 GeV) to detect a long-lasting (up to 200 s) high-energy (up to 4 GeV) emission. The analysis and interpretation

Table 1
LAT Time-resolved Spectroscopy

Time Bins (s)	Energy Index	Photon Flux Above 100 MeV ($\text{ph cm}^{-2} \text{s}^{-1}$)
(1) 0.38–0.48	$0.85^{+0.26}_{-0.30}$	$2.49^{+1.13}_{-0.84} 10^{-2}$
(2) 0.48–0.92	$1.20^{+0.20}_{-0.22}$	$1.80^{+0.46}_{-0.39} 10^{-2}$
(3) 0.92–1.5	$0.93^{+0.26}_{-0.30}$	$5.7^{+2.4}_{-1.8} 10^{-3}$
(4) 1.5–2.5	$1.41^{+0.28}_{-0.31}$	$6.4^{+2.0}_{-1.6} 10^{-3}$
(5) 2.5–5.5	$0.76^{+0.22}_{-0.26}$	$8.4^{+3.6}_{-2.7} 10^{-4}$
(6) 5.5–11.5	$0.86^{+0.35}_{-0.44}$	$2.0^{+1.4}_{-0.9} 10^{-4}$
(7) 11.5–37.0	$2.27^{+0.59}_{-0.70}$	$1.67^{+0.82}_{-0.59} 10^{-4}$
(8) 37.0–69.5	$0.85^{+0.32}_{-0.39}$	$4.4^{+2.6}_{-1.8} 10^{-5}$
(9) 69.5–200.0	$1.74^{+0.58}_{-0.71}$	$1.6^{+1.0}_{-0.7} 10^{-5}$
(10) 200–400	1.1/0.5/2.5	$< 4.7/3.2/7.9 10^{-6}$
(11) 400–800	1.1/0.5/2.5	$< 2.3/1.6/3.9 10^{-6}$
(12) 800–1500	1.1/0.5/2.5	$< 2.1/1.2/3.8 10^{-6}$
(13) 4200–7200	1.1/0.5/2.5	$< 0.48/0.3/1.0 10^{-6}$
(14) 10150–13000	1.1/0.5/2.5	$< 0.47/0.3/0.9 10^{-6}$
(15) 15800–18500	1.1/0.5/2.5	$< 0.52/0.3/1.0 10^{-6}$

Notes. No signal is detected in the LAT after T+200 s, and 95% confidence level upper limits on the flux are quoted for different assumptions of the energy index.

of the prompt emission will be presented in A. A. Abdo et al. (2010, in preparation). Follow-up observations lasted until 1500 s, when the source was occulted by the Earth, and resumed ~ 3.5 ks later.

The observation epochs are defined in Table 1. All analyses of LAT data follow the methodology described in Abdo et al. (2009). The results of the time-resolved spectroscopy are presented in Table 1. The spectrum shows no significant evolution, and it is well fitted by a power law with energy index $\beta_{\gamma} = 1.1 \pm 0.1$.

The burst onset in the GBM (T+0.013 s) tags the beginning of the emission bulk and is a sensible reference for the temporal fit. The light curve shows no significant features and is well fitted by a power law with a decay index $\alpha_{\gamma} = 1.38 \pm 0.07$ ($\chi^2/\text{dof} = 9.4/7$) (Figure 1).

3. DISCUSSION

GRB090510 was a short burst with a relatively bright afterglow, and E_{iso} is among the highest for this class (Graham et al. 2009). The early rise of the optical flux is so far unique in short GRBs. More importantly, GRB090510 shows high-energy emission up to the GeV range, until T+200 s.

Energetic short GRBs with optical transients, such as GRB050724 (Barthelmy et al. 2005b), typically have extended emission (EE) detected by BAT and XRT, following the hard emission spike (Troja et al. 2008). If GRB090510 had occurred at $z = 0.26$, as GRB050724, it would have produced a flux in the BAT range of a few 10^{-9} erg $\text{cm}^{-2} \text{s}^{-1}$ until ~ 100 s, and we would have classified it as an EE-GRB.

The nature of this high-energy emission is nevertheless not easy to understand. EE often fades slowly for a few hundreds of seconds, then vanishes with a slope which can be as fast as $\alpha \sim 7$; after this sudden drop a late afterglow with a typical decay slope $\alpha \sim 1.4$ is sometimes observed (e.g., GRB050724; GRB080123; Mangano et al. 2008). The fast decay and the extrapolation of the late afterglow back to early epochs suggest that EE is not the onset of the late afterglow (Nakar 2007). Furthermore, in a few cases where the EE is bright enough to be

studied in detail (Norris & Bonnell 2006), it shows variations too rapid to be explained with external shock models (Mészáros & Rees 1993). EE might instead indicate a declining activity of the GRB central engine (Rosswog 2007; Metzger et al. 2008; Perna et al. 2006; Goad et al. 2007); once this activity ends, then falls abruptly, and the forward shock (FS) emission prevails. In other cases, however, the flux decay from the beginning of *Swift* observations seems due to the usual FS mechanism, such as in GRB051221 (Burrows et al. 2006) and GRB 061201 (Stratta et al. 2007).

We propose and discuss two scenarios to explain the emission after the initial spike: in the first one, the emission is due to both external FS and internal shock (IS; Rees & Mészáros 1994) while in the second the emission is due to FS alone.

3.1. X-ray Internal Shock, Optical External Shock

In the first scenario, we assume that the initial X-ray (until the break at ~ 1.4 ks) and γ -ray fluxes are IS emission, while the FS is responsible for the optical light curve and the late X-ray flux. In particular, the optical rise may be due to the onset of FS emission, detected 10^2 – 10^3 s after the trigger in long GRBs (Oates et al. 2009), when the mildly relativistic reverse shock crosses the ejecta. This model can explain the different behavior of the early X-ray/LAT and optical light curves.

We constrain some physical properties of the FS blast wave by assuming that it propagates in a homogeneous medium. The initial Lorentz factor of the ejecta is about twice its value at the peak time and is estimated to be $\Gamma_0 = 1.4 \times 10^2 E_{53}^{1/8} n^{-1/8} t_{\text{peak},3}^{-3/8}$ (Sari 1997; Panaitescu & Kumar 2000), where E is the isotropic kinetic energy, n is the environment density in cm^{-3} , and t_{peak} is the peak time. The maximum FS flux is at the synchrotron characteristic frequency ν_m , and is $F_{\nu_m} = 1.3 \times 10^4 E_{53} \epsilon_{B,-2}^{1/2} n^{1/2} \mu\text{Jy}$ (Granot & Sari 2002), where ϵ_B is the fraction of internal energy in the magnetic field.

These parameter values must be consistent with $\Gamma_0 \gtrsim 1000$ (A. A. Abdo et al. 2010, in preparation) and with the UVOT data, which give a 3σ lower limit on $t_{\text{peak}} > 730$ s and a peak flux $F \simeq 100 \mu\text{Jy}$. The first constraint can be written as $E_{53} n^{-1} > 2.6 \times 10^6$. If ν_m is just below the optical band, the constraint on the flux becomes $E_{53} \epsilon_{B,-2}^{1/2} n^{1/2} \simeq 7.7 \times 10^{-3}$. Assuming $\epsilon_{B,-2} \simeq 1$, the model is consistent with observations for $E_{53} \gtrsim 5.4$, while $n \simeq 5.9 \times 10^{-5} E_{53}^{-2}$.

The XRT and LAT fluxes can be explained by IS synchrotron emission with $\nu_c < \nu_{\text{Opt}} < \nu_{\text{sa}} < \nu_X < \nu_m$, where ν_c is the synchrotron cooling frequency and ν_{sa} is the synchrotron self-absorption frequency (Guetta & Granot 2003). The synchrotron luminosity, estimated from the 100 s spectral energy distribution (SED; Figure 2), is $L \simeq 10^{50} \text{ erg s}^{-1}$. We find that for this value of L and for $p = 2.4$, $\epsilon_{e,-1} = 5.5$, $\epsilon_{B,-2} = 33$, $\Gamma = 410$, $t_v = 3 \times 10^{-5}$ s, where p , ϵ_e , Γ , and t_v are the index of the power-law electron energy distribution, the fraction of energy given to electrons, the bulk Lorentz factor, and the variability timescale, respectively, we have $\nu_m \simeq 210$ keV, $F(1.7 \text{ keV}) \simeq 75 \mu\text{Jy}$, which is within a factor of ~ 3 from the observations, and $F(100 \text{ MeV}) \simeq 4.2 \times 10^{-3} \mu\text{Jy}$, which is consistent within 2σ of the data. The cutoff energy for pair production is $h\nu_{\gamma\gamma} \simeq 1.6$ GeV, thus allowing the late emission of ~ 1 GeV photons. IS does not produce detectable emission in the optical, since this is below $\nu_{\text{sa}} \simeq 0.32$ keV.

Compared with the scenario presented in Section 3.2, this model has the advantage of not requiring extreme values of Γ_0 (e.g., > 5000) to explain an early (few seconds) FS emission

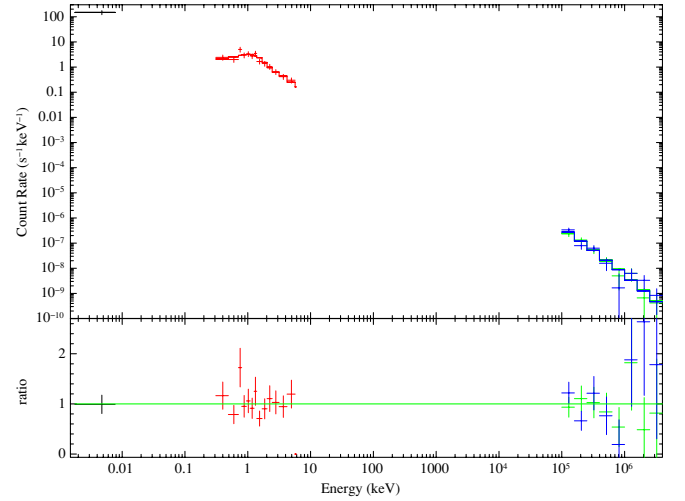


Figure 2. Broadband count spectrum at T+100 s, using UVOT (black), XRT (red), LAT front (green), and LAT back (blue) events data. The best fit and the residuals are shown (see the text).

onset in a low-density environment expected for a short burst. However, it needs some fine tuning of parameters. The optical rise slope $\alpha_{\text{Opt},1} = -0.5$ is shallower than that expected at the FS onset ($\alpha = -2$), although similar slow rises have been observed (Oates et al. 2009). It is possible that the onset of our observations caught the end of this steep rise phase, when the afterglow was turning over to a decay. Another possible problem is that the required density appears very low. We note that the observed slope would be expected if ν_m were crossing the optical band, and, in general, broad FS onset rises are also expected for outflows observed off-axis (Panaitescu & Verstrand 2008). However, a bright and hard event such as GRB090510 is difficult to reconcile with the latter scenario, which predicts soft and dim prompt emission (Yamazaki et al. 2002).

3.2. Optical, X-ray, and GeV Emission from External Shock

A second possibility is that the afterglow of GRB090510, including the emission detected by LAT, is entirely produced by the FS propagating in a constant density medium (Sari et al. 1998). According to the model, the broad afterglow spectrum⁶⁷ consists of three segments: a low-energy tail, of spectral slope $\beta_1 = -1/3$; another segment, for $\nu_m < \nu < \nu_c$, where $\beta_2 = (p - 1)/2$; a third segment, blueward of ν_c , with $\beta_3 = p/2$. For comparison with this spectral template, we produced 5 SEDs, at 100 s, 150 s, 1 ks, 7 ks, and 12 ks (Figure 3), all including UVOT and XRT data, and LAT data were also included in the first SED. LAT data were accumulated between 10 s and 200 s (i.e., well after the end of the prompt emission seen in the GBM) and renormalized to 100 s using the decay index of $\alpha_\gamma = 1.38$. We fitted the SEDs simultaneously with a double broken power-law model, forcing $\beta_1 = -1/3$ and $\beta_3 = \beta_2 + 1/2$. We allowed the breaks to vary, and Galactic and host extinction were accounted for. The result is acceptable ($\chi^2/\text{dof} = 110.3/83$) and is shown in Figure 3 and Table 2. The FS alone could successfully describe the spectrum over nine decades of frequency. A break between X-ray and γ -ray ranges is fitted, at $E_2^b \simeq 300$ MeV, but not constrained. It is studied more precisely by fitting the 100 s SED alone, freezing N_H and $E(B - V)$ at the 5 SEDs fit results and leaving β_2 and β_3 free to vary (see Table 2). This fit fulfills the relation $\beta_3 = \beta_2 + 1/2$

⁶⁷ The self-absorption frequency is not relevant in this study.

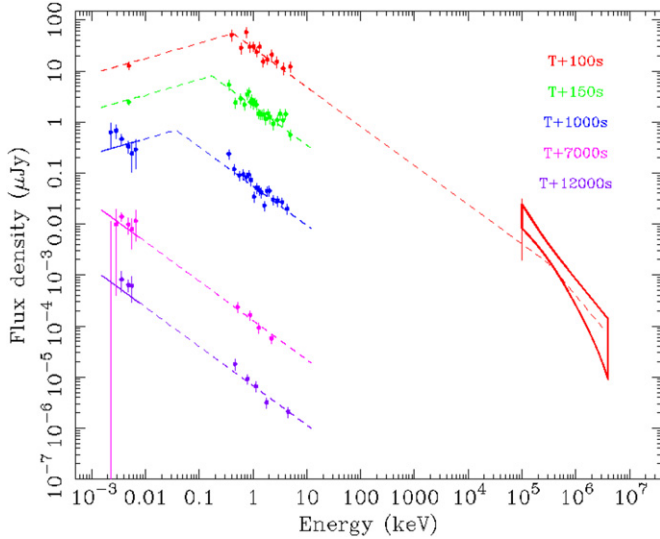


Figure 3. UVOT–XRT–LAT SEDs at different epochs, with the best fit shown (see the text). The butterfly at T+100 s indicates the 68% confidence level region for the LAT flux (95% error bar at 100 MeV is shown). Successive SEDs in time order are rescaled by 1:1, 1:10, 1:100, 1:1000, 1:10,000.

(at 1.3σ) and a significant break is found (3.6σ), although it yields a slightly harder β_2 (1.8σ) than the 5 SED fit shown in Figure 3. The LAT emission shows no spectral evolution, even at early times. Therefore, to better characterize the high-energy spectrum, the SED at 100 s was rebuilt including LAT data between 0.38 s and 200 s (see Table 2 and Figure 2). A significant break ($>4.5\sigma$ including systematics) between 10 and 133 MeV was found. However, including this selection of LAT data in the 5 SED fit yields a worse fit ($\chi^2/\text{dof} = 125.3/83$) than that shown in Figure 3.

In this FS interpretation, the initial increase of the optical emission is due to ν_m approaching the optical band. The X-ray is already decaying because it lies above ν_m . In order to verify whether the required physical parameters are plausible, we impose the following constraints: (1) $F(1 \text{ ks}) \simeq 2.2 \mu\text{Jy}$ at 10^{18} Hz and (2) $\nu_m(1 \text{ ks}) \simeq 10^{16} \text{ Hz}$. Adopting the expressions for F_{ν_m} , ν_m , and ν_c from Granot & Sari (2002), the constraints become

$$\epsilon_{B,-2} \simeq 14 E_{53}^{-1} \epsilon_{e,-1}^{-4} \xi_p^{-4} \nu_{os}^2 \quad (1)$$

$$n \simeq 1.5 \times 10^{-6} (100)^{p-2.5} E_{53}^{-1} \epsilon_{e,-1}^4 \xi_p^4 \nu_{os}^{-p-1}, \quad (2)$$

where $\xi_p = 3(p-2)/(p-1)$ and $\nu_{os} = \nu_m(1 \text{ ks})/10^{16} \text{ Hz}$. We verified that the synchrotron self-Compton cooling is not significant for $t \leq 1.5 \text{ ks}$ and $\nu_c(1.5 \text{ ks}) > 10^{18} \text{ Hz}$ for a reasonable range of parameters (Nakar et al. 2009). A very low, but not implausible, density is suggested.

The flux at 100 MeV is

$$F_{\nu > \nu_c} \simeq 2.4 \times 10^{-3} (3.6 \times 10^{-3})^{(p-2.5)} E_{53} \epsilon_{e,-1} (t/100 \text{ s})^{(2-3p)/4} \times (h\nu/100 \text{ MeV})^{-p/2} \xi_p \nu_{os}^{(p-2)/2} \mu\text{Jy}. \quad (3)$$

This is consistent with the LAT data at 100 s, provided $E_{53} \epsilon_{e,-1} \simeq 5$, $p \approx 2.5$, $\xi_p \approx 1$, and $\nu_{os} \approx 1$. For these parameters, $\nu_c \ll 4 \text{ GeV}$ at $t \gtrsim 1 \text{ s}$, so that the flux in the LAT energy range is approximately $F \propto t^{(2-3p)/4} \sim t^{-1.4}$ at $t \gtrsim 1 \text{ s}$, consistent with the LAT light curve. We note that $\Gamma_0 > 5800 E_{53}^{1/8} n^{-1/8}$ is required for the FS onset time to be $\lesssim 1 \text{ s}$.

Table 2

Best-Fit Parameters Obtained by Fitting the 5 SEDs Simultaneously or the SED at 100 s Only with a Double Broken Power-Law Model

SED	5 SEDs (10–200)	100 s (10–200)	100 s (0.38–200)
LAT Data Set (s)			
N_H ($\times 10^{21} \text{ cm}^2$)	$1.52^{+0.33}_{-0.30}$	1.52 (fixed)	1.52 (fixed)
$E(B-V)$ (mag)	$0.000^{+0.005}_{-0.000}$	0. (fixed)	0. (fixed)
E_1^b (keV)	$0.43^{+0.10}_{-0.07}$ (100 s)		
	$0.17^{+0.03}_{-0.02}$ (150 s)		
	$0.037^{+0.005}_{-0.007}$ (1000 s)	$0.31^{+0.05}_{-0.06}$	$0.31^{+0.06}_{-0.05}$
	<0.001 (7000 s)		
	<0.01 (12000 s)		
β_2	0.77 ± 0.04	$0.61^{+0.06}_{-0.10}$	$0.62^{+0.08}_{-0.06}$
E_2^b (MeV)	$\simeq 300$ (100 s)	[20–135]	[10–133]
β_3	$\beta_2 + 1/2$	$1.44^{+0.26}_{-0.22}$	$1.14^{+0.10}_{-0.09}$

Notes. N_H and $E(B-V)$ are host absorption and extinction, respectively; E_1^b and E_2^b are the two break energies calculated at the epoch in parentheses.

In summary, the spectral properties of GRB 090510 could be explained by a simple FS model. We note, though, that this model is hard to reconcile with some of the observed temporal properties. First, it predicts an X-ray decay index before the break of $\alpha = 3\beta_2/2 = 1.16 \pm 0.06$, clearly inconsistent with the observed $\alpha_{X,1} = 0.74 \pm 0.03$. Second, if the X-ray break at $t = 1.4 \text{ ks}$ is attributed to a jet break (Sari et al. 1999) and, after this time, optical and X-ray lie on the same spectral segment, then the asymptotic optical decay index should be consistent with $\alpha_{X,2} = 2.18 \pm 0.10$. However, a fit of the whole light curve with a smooth broken power law (Section 2.3), adding a constant (as a host galaxy contribution), gives an asymptotic decay slope $\alpha_{\text{Opt},2} = 1.13^{+0.17}_{-0.09}$, incompatible with the X-ray decay. Finally, although the error bars are quite large, we note that, taken at face value, the slope of the UVOT spectrum in the 1 ks SED is negative (Figure 3), suggesting that ν_m may already be below the optical at that epoch.

The above-mentioned flaws imply that the simple FS model is not viable to explain the properties of GRB090510. However, this model relies on highly idealized assumptions, and it is known that several GRB afterglows do not strictly follow its simple predictions. Plausible effects that may affect the predictions and ease the comparison with GRB090510 are as follows:

1. A phase of energy injection (Sari & Mészáros 2000), or an evolution of the microphysical parameters of the blast wave (Panaitescu et al. 2006); both may cause an early shallow decay of the X-ray flux.
2. The transit of ν_m slightly after the jet break, which could explain a shallow late optical decay.

With the present data, we are unable to distinguish between energy injection and microphysical parameter evolution. As for the X-ray decay post jet break, hydrodynamical simulations show that the jet decay slope can temporarily reach $\alpha \simeq 3$ (Granot 2007). Both the processes of energy injection and parameter evolution are capable of keeping the decay shallower, so that a late X-ray decay slope of $\alpha_{X,2} = 2.18 \pm 0.10$ could be achieved. Therefore, with some extensions, the FS model could arrange the temporal properties, although some fine tunings would be needed.

4. CONCLUSIONS

We have reported the *Swift* and *Fermi* observations of the short GRB090510, an event endowed with bright prompt and afterglow emission, and detected in the GeV range up to 200 s after the trigger. The initial X-ray emission shows a slow decay up to $\simeq 1.4$ ks, after which it quickly drops. The optical flux peaks at $\simeq 1.6$ ks. We have explored two scenarios to explain the observed behaviors.

In the first scenario, the early flux detected by XRT and LAT is due to IS, while the optical rise is the onset of FS emission or the transit of v_m . This interpretation does not require extremely high values of Lorentz factor, should the density of the environment be very low. We also find that reasonable values for the physical parameters can lead to the observed properties, which might favor the model, although some fine tuning is necessary. The second scenario assumes that the FS produces the full spectrum of the emission, observed from the optical to the GeV band. The γ -ray, X-ray, and optical spectrum can be reproduced by the template FS spectral model, and the required physical parameters are plausible. Although the simple FS model fails to reproduce the observed temporal behavior, extensions of this model could accommodate the temporal mismatch. In order to identify the origin of the GeV component of GRBs like 090510, more case studies will be necessary. Fortunately, we have very promising prospects for other simultaneous *Fermi* and *Swift* observations of short GRBs, which will provide us with more measurements to shed light on the properties of these events.

The *Fermi* LAT Collaboration acknowledges support from a number of agencies and institutes for both development and the operation of the LAT as well as scientific data analysis. These include NASA and DOE in the United States, CEA/Irfu and IN2P3/CNRS in France, ASI and INFN in Italy, MEXT, KEK, and JAXA in Japan, and the K. A. Wallenberg Foundation, the Swedish Research Council and the National Space Board in Sweden. Additional support from INAF in Italy and CNES in France for science analysis during the operations phase is also gratefully acknowledged. S.Z. acknowledges STFC support. This work used data supplied by the UK Swift SDC at the University of Leicester.

REFERENCES

- Abdo, A. A., et al. 2009, *ApJ*, 707, 580
 Barthelmy, S. D., et al. 2005a, *Space Sci. Rev.*, 120, 143
 Barthelmy, S. D., et al. 2005b, *Nature*, 438, 944
 Beuermann, K., et al. 1999, *A&A*, 352, 26
 Burrows, D. N., et al. 2005, *Space Sci. Rev.*, 120, 165
 Burrows, D. N., et al. 2006, *ApJ*, 653, 468
 Evans, P. A., et al. 2007, *A&A*, 469, 379
 Evans, P. A., et al. 2009, *MNRAS*, 397, 1177
 Ferrero, P., et al. 2006, *A&A*, 457, 857
 Fong, W., Berger, E., & Fox, D. B. 2010, *ApJ*, 708, 9
 Gehrels, N., Ramirez-Ruiz, E., & Fox, D. S. 2009, *ARA&A*, 47, 567
 Gehrels, N., et al. 2004, *ApJ*, 611, 1055
 Goad, M. R., et al. 2007, *A&A*, 468, 103
 Graham, J. F., et al. 2009, *ApJ*, 698, 1620
 Granot, J. 2007, *RevMexAA (Conf. Ser.)*, 27, 140
 Granot, J., & Sari, R. 2002, *ApJ*, 568, 820
 Guetta, D., & Granot, J. 2003, *ApJ*, 585, 885
 Guiriec, S., Connaughton, V., & Briggs, M. 2009, GCN Circular, 9336, 1
 Hoversten, E. A., et al. 2009, GCN Circular, 9331, 1
 Kouveliotou, C., et al. 1993, *ApJ*, 413, L101
 Mangano, V., et al. 2008, GCN Circular, 7208, 1
 Mészáros, P., & Rees, M. 1993, *ApJ*, 405, L278
 Metzger, B. D., Quataert, E., & Thompson, T. A. 2008, *MNRAS*, 385, 1455
 Nakar, E. 2007, *Phys. Rep.*, 442, 166
 Nakar, E., Ando, S., & Sari, R. 2009, *ApJ*, 703, 675
 Norris, J. P., & Bonnel, J. T. 2006, *ApJ*, 643, 266
 Oates, S. R., et al. 2009, *MNRAS*, 395, 490
 Ohno, M., & Pelassa, V. 2009, GCN Circular, 9334, 1
 Panaitescu, A., & Kumar, P. 2000, *ApJ*, 543, 66
 Panaitescu, A., & Vestrand, T. 2008, *MNRAS*, 387, 479
 Panaitescu, A., et al. 2006, *MNRAS*, 369, 2059
 Perna, R., Armitage, P. J., & Zhang, B. 2006, *ApJ*, 636, L29
 Poole, T. S., et al. 2008, *MNRAS*, 383, 627
 Rau, A., et al. 2009, GCN Circular, 9353, 1
 Rees, M. J., & Meszaros, P. 1994, *ApJ*, 430, L93
 Roming, P. W. A., et al. 2005, *Space Sci. Rev.*, 120, 95
 Rosswog, S. 2007, *RevMexAA (Conf. Ser.)*, 27, 57
 Sari, R. 1997, *ApJ*, 489, L37
 Sari, R., & Mészáros, P. 2000, *ApJ*, 535, L33
 Sari, R., Piran, T., & Helpert, J. 1999, *ApJ*, 519, L17
 Sari, R., Piran, T., & Narayan, R. 1998, *ApJ*, 497, L17
 Spergel, D. N., et al. 2003, *ApJS*, 148, 175
 Stratta, G., et al. 2007, *A&A*, 474, 827
 Troja, E., et al. 2008, *MNRAS*, 385, 10
 Ukwatta, T. N., et al. 2009, GCN Circular, 9337, 1
 Yamazaki, R., Ioka, K., & Nakamura, T. 2002, *ApJ*, 571, L31
 Zhang, B., et al. 2009, *ApJ*, 703, 1696